Nat. Hazards Earth Syst. Sci. Discuss., 2, 2981–3013, 2014
www.nat-hazards-earth-syst-sci-discuss.net/2/2981/2014/
doi:10.5194/nhessd-2-2981-2014

Natural Hazards and Earth System Sciences
Open Access
Discussions

Signatures of the self-affinity of fracture and faulting in pre-seismic electromagnetic emissions

S. M. Potirakis[1], K. Eftaxias[2], G. Balasis[3], J. Kopanas[2], G. Antonopoulos[4], and A. Kalimeris[4]

[1]Department of Electronics Engineering, Technological Education Institute (TEI) of Piraeus, 250 Thivon & P. Ralli, 12244, Aigaleo, Athens, Greece
[2]Department of Physics, Section of Solid State Physics, University of Athens, Panepistimiopolis, 15784, Zografos, Athens, Greece
[3]Institute for Astronomy, Astrophysics, Space Applications and Remote Sensing, National Observatory of Athens, I. Metaxa & Vas. Pavlou St., 15236 Penteli, Greece
[4]Department of Environmental Technology and Ecology, Technological Education Institute (TEI) of the Ionian Islands, Panagoulas road, 29100, Zante, Greece

Received: 14 January 2014 – Accepted: 14 April 2014 – Published: 30 April 2014

Correspondence to: K. Eftaxias (ceftax@phys.uoa.gr)

Published by Copernicus Publications on behalf of the European Geosciences Union.

Abstract

Of particular interest is the detection of precursors of an impending rupture. Theoretical, numerical studies along with laboratory experiments indicate that precursory signs of an impending failure are the sudden drop of fractal dimension and entropy, along with the anticorrelated, for large system sizes, rising of Hurst exponent and drop of a frequency–size power-law scaling exponent. Based on the widely accepted concept of the self-affine nature of faulting and fracture, we examine whether these precursory signs exist in the fracto-electromagnetic emissions resulting from the activation of a single fault.

1 Introduction

Understanding how materials break is a fundamental problem that has both theoretical and practical importance (Girard et al., 2012). During the past two decades, considerable effort has been devoted by scientists to the study of damage and fracture in heterogeneous media (e.g., rocks) (Herrmann and Roux, 1990; Sornette, 2000). Of particular interest is the detection of precursors of an impending rupture. Laboratory studies have detected various precursory signatures of an impending failure (Ponomarev et al., 1997; Sornette, 2000; Rabinovitch et al., 2001; Bahat et al., 2005; Hadjicontis et al., 2007; Carpinteri et al., 2009a, 2009b; Hadjicontis et al., 2011; Kuksenko et al., 2011; Vettegren et al., 2012). Theoretical and numerical studies have devoted efforts for the explanation of the experimental precursory signs and suggested new ones (e.g., Bouchaud, 1997; Guarino et al., 2002; Rundle et al., 2003; Sahimi and Tajer, 2005; Uyeda, 2009).

Earthquakes (EQs, see Table 1 for a full list of acronyms/abbreviations) are large-scale fracture phenomena in the Earth's heterogeneous crust. Since the early work of Mandelbrot (1983), the self-affine nature of faulting and fracture is widely documented from the analysis of data both field observations and experiments (Sornette, 2000 and

NHESSD
2, 2981–3013, 2014

references therein). The question naturally arising is whether the precursory signs reported by laboratory, theoretical and numerical studies are also extended to the activation of a single fault. Herein we focus on this point, checking for compatibility with the following three points.

1. Theoretical studies performed by Lu et al. (2005) found that the Fractal Dimension (FD) and entropy decreases as the damage in a disordered media evolves. A sudden drop of FD might be viewed as a likely precursor prior to a final catastrophic failure.

2. Long-range connective sandpile (LRCS) models (Lee et al., 2009; Chen et al., 2011; Lee et al., 2012) predict a negative correlation between Hurst exponent H (see Table 2 for a full list of symbols) and a frequency–size power-law scaling exponent B (or the FD) for large system sizes. These seem to be consistent with studies of earthquake fault systems and real seismicity data (Frankel, 1991; Hallgass et al., 1997; Chen et al., 2011; Lee et al., 2012); the B values (and FD) typically reduce prior to large avalanches, which mimics the observed precursory phenomena of the Gutenberg–Richter b values in real seismicity, while the H values increase.

3. A self-affine model (SAM) for the seismicity that mimics the fault friction by means of two fractional Brownian profiles that slide one over the other has been introduced by Hallgass et al. (1997). An earthquake occurs when there is an overlap of the two faces and its energy is assumed proportional to the overlap surface. The SAM exhibits the dependence of the Gutenberg–Richter law exponent to the roughness, H, of the fault surface profiles. More precisely, in their numerical simulations they observed that the probability of an earthquake releasing an energy ε, $P(\varepsilon)$, is following the power law $P(\varepsilon) \propto \varepsilon^{-1-\gamma}$, where $\gamma = 1 - H/(d-1)$ in the general d-dimension case.

Finally, we check whether laboratory results are also compatible with the corresponding ones rooted in the activation of a single fault.

NHESSD
2, 2981–3013, 2014

The activation of a single fault has been suggested that can be monitored through the observation and analysis of fracture-induced electromagnetic (EM) emissions in the MHz and kHz frequency bands according to a three stage model (see Sect. 2). Since, according to the specific model, the kHz EM emissions are considered to stem from the last stage of the EQ preparation process, we are seeking for the above mentioned precursory signs in the kHz emissions.

Our analysis is performed by means of: (i) FD evolution, estimated through the Hurst exponent resulting from rescaled-range (R/S) analysis, detrended fluctuation analysis (DFA), and spectral power law analysis; (ii) universal roughness of fracture surfaces; (iii) Gutenberg–Richter frequency–magnitude exponent b evolution, calculated both directly and through the analysis in terms of a non-extensive model for earthquake dynamics and (iv) in terms of the recently proposed fuzzy entropy (FuzzyEn).

The results obtained after the analysis reveal good agreement to the corresponding theoretical, numerical and laboratory ones. The results indicate that the fracto-electromagnetic emissions associated with the activation of a single fault are compatible to the self-affine nature of fracture and faulting and provide clear indications that critical fracture is approaching.

2 Fracture-induced electromagnetic emissions

Crack propagation is the basic mechanism of material's failure. The motion of a crack has been shown to be governed by a dynamical instability causing oscillations in its velocity and structure on the fracture surface. Experimental evidence indicates that the instability mechanism is that of local branching: a multicrack state is formed by repetitive, frustrated microfracturing events (Sharon and Fineberg, 1999 and references therein).

Electromagnetic emissions in a wide frequency spectrum ranging from kHz to MHz are produced by cracks' opening, which can be considered as the so-called precursors of general fracture (Karamanos et al., 2006 and references therein). The radiated EM precursors are detectable both at laboratory (Nitsan, 1977; Rabinovitch et al., 2001;

NHESSD
2, 2981–3013, 2014

Bahat et al., 2005; Fukui et al., 2005; Hadjicontis et al., 2007, 2011; Lacidogna et al., 2011) and at geophysical scale (Warwick et al., 1982; Gokhberg et al., 1995; Kapiris et al., 2004a; Contoyiannis et al., 2005; Karamanos et al., 2006; Papadimitriou et al., 2008; Kalimeri et al., 2008; Eftaxias, 2011; Potirakis et al., 2012a, b). An important feature at laboratory scale is that the MHz radiation precedes the kHz one: the kHz EM emission is launched in the tail of pre-fracture EM emission from 97 % up to 100 % of the corresponding failure strength (Eftaxias et al., 2001 and references therein). *We note that an EM silence systematically emerges before the time of the EQ occurrence* (Gokhberg et al., 1995; Matsumoto et al., 1998; Hayakawa and Fujinawa, 1994; Hayakawa, 1999; Morgounov, 2001; Eftaxias et al., 2012, 2002 and references therein). Clear fracture-induced MHz–kHz EM precursors have been detected over periods ranging from approximately a week to a few hours prior to significant EQs (Eftaxias et al., 2001; Kapiris et al., 2004a; Contoyiannis et al., 2005; Karamanos et al., 2006; Papadimitriou et al., 2008; Kalimeri et al., 2008; Eftaxias, 2011; Potirakis et al., 2012a, b). Importantly, the MHz radiation precedes the kHz one as it happens at the laboratory scale (Eftaxias et al., 2001; Kapiris et al., 2004a; Contoyiannis et al., 2005; Karamanos et al., 2006; Papadimitriou et al., 2008; Kalimeri et al., 2008; Eftaxias, 2011; Potirakis et al., 2012a, b). The remarkable asynchronous appearance of these precursors indicates that they refer to different stages of the EQ preparation process. The following three stage model of EQ generation by means of pre-fracture EM activities has been proposed (Kapiris et al., 2004a; Contoyiannis et al., 2005; Eftaxias et al., 2013; Eftaxias and Potirakis, 2013):

(i) The pre-seismic MHz EM emission is thought to be due to the fracture of the highly heterogeneous system that surrounds the family of large high-strength entities distributed along the fault sustaining the system. It can be described as analogous to a thermal continuous phase transition, while a Levy-walk-type mechanism can drive the heterogeneous system to criticality.

NHESSD
2, 2981–3013, 2014

(ii) The final kHz EM radiation is due to the fracture of the aforementioned large high-strength entities themselves. A sequence of kHz EM pulses is emerged where there is an intersection between the two rough profiles of the fault. Note that laboratory experiments show that the kHz EM emissions are generally observed only in correspondence to sharp stress drops or the final collapse (Lacidogna et al., 2011), namely, they characterize the final stage of a fracture (Ohnaka and Mogi, 1982; Ohnaka, 1983; Krajcinovic, 1996; Lavrov, 2005; Mori and Obata, 2008; Soulioti et al., 2009; Lacidogna et al., 2010, 2011; Schiavi et al., 2011; Aggelis et al., 2011).

(iii) The systematically observed EM silence in all frequency bands is sourced in the stage of preparation of dynamical slip which results to the fast, even super-shear, mode that surpasses the shear wave speed (Eftaxias et al., 2013b).

The well documented fracture-induced kHz EM signal associated with the Athens EQ, with magnitude 5.9, occurred on 7 September 1999 (e.g. Kapiris et al., 2004a; Contoyiannis et al., 2005; Karamanos et al., 2006; Papadimitriou et al., 2008; Kalimeri et al., 2008; Potirakis et al., 2012a, b), is employed in this contribution as a test case. Part of the recorded time series covering 11 days period from 28 August 1999, 00:00:00 (UT), to 7 September 1999, 23:59:59 (UT), and containing the candidate precursor signal is shown in Fig. 1. Importantly, the two strong impulsive kHz electromagnetic (EM) bursts in the tail of the specific signal present compatibility with the radar interferometry data and the seismic data analysis, which indicates that two fault segments were activated during Athens EQ. The calculated Fisher information and approximate entropy content ratios closely follow the radar interferometry result that the main fault segment was responsible for 80 % of the total energy released, while the secondary fault segment for the remaining 20 % (Potirakis et al., 2012b).

The (left) vertical broken green line in Fig. 1 roughly indicates the start of the candidate precursor. Before that the recordings correspond to the background electromag-

NHESSD
2, 2981–3013, 2014

netic noise at the position of the station. The (right) vertical broken red line in Fig. 1 indicates where the damage evolution of the fault approaches the critical point.

3 Experimental data analysis

In the following we examine whether precursory characteristics predicted by theoretical, numerical studies and laboratory experiments are also included in fracture-induced EM emissions. First, we analyze the experimental data in terms of the Hurst exponent and the corresponding FD temporal evolution, by means of the rescaled-range (R/S) analysis, detrended fluctuation analysis (DFA), and spectral power law analysis. Then, we study the evolution of Gutenberg–Richter frequency–magnitude exponent, calculated both directly and through the analysis in terms of a non-extensive model for earthquake dynamics. Finally, the entropy evolution is examined by means of the FuzzyEn.

3.1 Hurst exponent

The rescaled range R/S analysis was chosen for the direct calculation of the Hurst exponent, while the DFA method, as well as the spectral power law method, were chosen for the indirect estimation of Hurst exponent under the fractional Brownian motion (fBm) model hypothesis, which is respectively checked for its validity.

The exponent H characterizes the persistent/anti-persistent properties. The range $0 < H < 0.5$ indicates anti-persistency, which means that if the fluctuations presently increase, it is expected to change tendency in near future (negative feedback mechanism). On the contrary, persistent behavior is characterized by $0.5 < H < 1$ and then the underlying dynamics is governed by a positive feedback mechanism. The employed methods for the calculation/estimation of H are briefly reviewed in the following.

The R/S analysis (Hurst, 1951; Mandelbrot and Wallis, 1968) is based on two quantities: first, the range R_n, which is the difference between the maximum and minimum

NHESSD
2, 2981–3013, 2014

values of the accumulated departure of the time series from the mean, calculated over each one ($n = 1, 2, \ldots, d$) of the m-samples long sub-series in which the time-series can be divided, and second, the standard deviation of the corresponding sub-series S_n. The so-called *rescaled range* is exactly the ratio of R by S. Hurst found that (R/S) scales by power-law as time (i.e., the sample length m of the sub-series) increases,

$$(R/S)_m \propto m^H, \tag{1}$$

where H is the Hurst exponent. The exponent H is estimated as the linear slope of a $\log(R/S)_m - \log m$ representation.

Detrended Fluctuation Analysis (DFA) is a straightforward technique for identifying the extent of fractal self-similarity in a seemingly non-stationary time-series (Peng et al., 1994, 1995). After dividing a time-series to sub-series of m-samples length, the root mean-square fluctuation for the integrated and detrended series, $F(m)$ is calculated. Repeating this calculation for different m, a power-law relation between $F(m)$ and time (expressed by sub-series length m)

$$F(m) \propto m^a \tag{2}$$

indicates the presence of scaling. The DFA exponent a is estimated as the linear slope of a $\log F(m) - \log m$ representation.

Moreover, if an observed time-series is a temporal fractal, it should follow a spectral power law

$$S(f) \propto f^{-\beta}, \tag{3}$$

where $S(f)$ is the power spectral density, and f the frequency. The spectral power law exponent is estimated as the linear spectral slope $-\beta$ of a $\log S(f) - \log f$ representation of the power spectrum. The quality of fit to spectral power-law (as well as for the power laws of the other two methods) is usually measured in terms of the linear correlation coefficient, r^2.

NHESSD
2, 2981–3013, 2014

The spectral scaling exponent β is related to the Hurst exponent, H:

$$\beta = 2H + 1, \quad (4)$$

with $0 < H < 1$ ($1 < \beta < 3$) for the fBm model (Heneghan and McDarby, 2000).

Moreover, the relations between the DFA exponent a, the Hurst exponent H, and the spectral power law exponent β in the case of an fBm time-series are (Buldyrev et al., 1995; Shadkhoo et al., 2009)

$$H = a - 1 \quad \text{and} \quad (5)$$

$$\beta = 2a - 1. \quad (6)$$

The Hurst exponent is first directly calculated using the R/S method, and the result is simply denoted by H in the following. Then the Hurst exponent is also estimated, under the fBm hypothesis, from the calculated DFA exponent a (using Eq. 5) and the spectral scaling exponent β (using Eq. 4), while the estimated Hurst exponents are denoted in the following as H_a and H_β, respectively, in order to be easily discriminated from the directly calculated, by the R/S method, H.

The R/S method Hurst exponent, H, and the DFA exponent, a, were calculated using on successive non-overlapping 1024 samples long windows, and running time average of four windows with 25 % overlapping. Only the exponent values which arose for fitting of correlation coefficient $r^2 > 0.85$ to the corresponding power laws were considered here. The resulting, H and H_a are depicted in Fig. 2b and c, respectively.

The spectral scaling exponent β was estimated by calculating the morlet wavelet spectrum on successive, overlapping, time-windows of 1024 samples width each, an overlap of 75 %, i.e., sliding with a step of 256 samples, and running time average of four windows with 25 % overlapping. Only the β exponent values which presented correlation coefficient $r^2 > 0.85$ were considered here. The results for the corresponding estimated H_β, resulting from β supposing an fBm model and therefore employing Eq. (4), are presented in Fig. 2d.

NHESSD
2, 2981–3013, 2014

First of all we focus on the validity of the fBm model hypothesis. We claim that the above results verify the validity of the fBm model hypothesis for the signal under analysis for the following two reasons: (i) the comparison among the differently calculated/estimated Hurst exponents reveal that all of them are consistent to each other. Note that, the estimated values are similar throughout the signal duration, i.e., to the right of the first (green) broken line; (ii) the calculated spectral scaling exponent values are within the frame of the expected, for fBm time-series, $1 < \beta < 3$ (Heneghan and McDarby, 2000). If the fBm hypothesis was not valid, then at least one of the two independent indirect methods for the estimation of the Hurst exponent, under the fBm hypothesis, should lead to different results from those obtained through its direct calculation by the R/S method. We note that during the last part of the analyzed time-series, following the right (red) vertical broken line, the two strong EM bursts follow the persistent ($H > 0.5$) fBm model.

Fracture surfaces have been found to be self-affine following the fractional Brownian motion (fBm) model over a wide range of length scales. Specifically, they are characterized by $H \sim 0.7$–0.8, weekly dependent on the failure mode and the nature of the material, leading to the interpretation that this range of Hurst exponent values constitute a universal indicator of surface fracture (Lomnitz, 1994; Lopez and Schmittbuhl, 1998; Hansen and Schmittbuhl, 2003; Zapperi et al., 2005; Ponson et al., 2006; Mourot et al., 2006).

According to our three-stage model (see Sect. 2), the kHz EM radiation is due to the interaction of the two rough profiles of the fault. Therefore, it is expected that the roughness of the analyzed kHz time-series, should be consistent to the global values of fault roughness. Indeed, all the estimated Hurst exponent values during the two strong EM bursts converge to $H \sim 0.7$.

As recently pointed out in Chen et al. (2011) and Lee et al. (2012), Hallgass et al. (1997) have introduced a self-affine model (SAM) for the seismicity that mimics the fault friction by means of two fractional Brownian profiles that slide one over the other. Since the roughness index, H, of the analyzed EM time series is $H \sim 0.7$, the

NHESSD
2, 2981–3013, 2014

SAM predicts that the probability an EM pulse having an energy ε should be denoted by $P(\varepsilon) \propto \varepsilon^{-1-\gamma}$, where $\gamma = 1 - H = 0.3$ and thus $P(\varepsilon) \propto \varepsilon^{-1.3}$, given that the EM time-series is a two-dimensional variation, i.e. $d = 2$. The question arises whether the energy of EM pulses follow the power law $P(\varepsilon) \propto \varepsilon^{-1.3}$. Indeed, the cumulative distribution function of the specific EM time-series amplitudes has been proved to follow the power law $N(> A) \sim A^{-0.62}$ (Kapiris et al., 2004b), and, consequently, the distribution function of the energies follows the power-law $P(\varepsilon) \sim \varepsilon^{-1.31}$ (Maes et al., 1998). It is noted that Petri et al. (1994) found a power-law scaling behavior in the acoustic emission energy distribution with $-1 - \gamma = -1.3 \pm 0.1$. Houle and Sethna (1996) found that the crumpling of paper generates acoustic pulses with a power-law distribution in energy with $-1 - \gamma \in (-1.6, -1.3)$. On the other hand, Cowie et al. (1993), Sornette et al. (1994), and Cowie et al. (1995), have developed a model of self-organized EQs occurring on self-organized faults. Their theoretical study suggests that the corresponding exponent value should be $-1 - \gamma = -1.3$.

Finally, a physical modeling of the formation and evolution of seismically active fault zones has been studied in the frame of laboratory experiments which also ended-up to compatible values of Hurst exponents ($H \sim 0.7$) for both space and time analysis (Ponomarev et al., 1997), which is also in agreement with the obtained results for the kHz EM time-series.

The above results on Hurst exponent are consistent both to the numerical results for the LRCS model (Lee et al., 2009, 2012; Chen et al., 2011), predicting increase of Hurst exponent prior to large events, and the SAM model (Hallgass et al., 1997), yielding an energy distribution exponent very close to the predicted by the model and past laboratory experiments.

3.2 Fractal dimension

Given the validity of the fBm model hypothesis, the Hausdorff–Besicovitch FD D_h can be estimated from the relation (Lowen and Teich, 1995; Heneghan and McDarby,

NHESSD
2, 2981–3013, 2014

2000)

$$D_h = 2 - H = (5 - \beta)/2. \quad (7)$$

The corresponding FD values resulting from the directly calculated (R/S) Hurst exponent, H, and the estimated from the calculated DFA exponent a, H_a, and the spectral scaling exponent β, H_β, are in that order denoted by D_h, D_{ha} and $D_{h\beta}$. The analysis results are depicted in Fig. 3b–d, respectively.

From Fig. 3 it is apparent that all the estimated FDs suddenly drop during the two strong EM pulses, compared to the background noise as well as to the first part of the signal (the part between the green – left – and red – right – broken vertical lines). Note that all of them reach values of $D_h \sim 1.3$ during these two strong pre-EQ EM emissions. These results are consistent to theoretical findings of Lu et al. (2005), predicting sudden drop of FD prior to the final catastrophic failure. Moreover, the sudden drop of FD has also been observed in laboratory experiments (Ponomarev et al., 1997), while the FD value yielded for the EM signal under analysis is also consistent to the corresponding of the geophysical scale, obtained for distribution of rupture fault lengths irrespective of their positions (Sornette, 1991; Kapiris et al., 2004b). This, for a single major fault, has been estimated to $D \sim 1.2$ by seismological measurements as well as theoretical studies (e.g. Sahimi, 1993; Sahimi et al., 1993, and references therein).

The direct calculation of the FD for the signal of Fig. 1 has already been presented in (Potirakis et al., 2012c), in terms of the box-counting and the Higuchi's algorithms, giving a FD ~ 1.6 during the two strong EM pulses. These two methods are also successfully highlighting the sudden drop of fractal dimension prior to the final catastrophic failure in agreement to the theoretical findings of Lu et al. (2005).

Nevertheless, we observe a difference between the results of Potirakis et al. (2012c) and the indirectly estimated FD of Fig. 3 as a result of the sensitivity of the box-counting and the Higuchi's algorithms to noise. It is a common knowledge that all practical FD estimates are very sensitive to numerical or experimental noise (e.g. Raghavendra and Narayana Dutt, 2010). The presence of noise leads to FD estimates which are higher

NHESSD
2, 2981–3013, 2014

than the actual FD. Since the field-acquired EM time series under analysis is certainly contaminated by measurement noise, the calculated FD values were higher than the actual, while the different sensitivity to the measurement noise led to differences between the FD estimates through the two algorithms employed in Potirakis et al. (2012c). Although various algorithms for calculating FD have been developed, a general solution is not available. It is often said (e.g. Schmittbuhl et al., 1995), that at least two different algorithms are needed for a faithful representation of the FD of a time series.

However, the indirect estimation presented here (Fig. 3) through three different methods led to similar results. Therefore, provided the proven validity of the considered fBm model, as well as the consistency of the resultant Hurst exponent values with the corresponding numerical model and laboratory facts, one could end-up to the conclusion that the Hurst exponent sourced FDs have to be considered more reliable than the ones calculated by the Higuchi or the box-counting methods, which are probably prone to higher FD values than the actual ones due to measurement noise.

3.3 Frequency–size law

Earthquake dynamics have been found to follow the frequency–magnitude scaling relation, known as Gutenberg–Richter law (Gutenberg and Richter, 1954)

$$\log N(>M) \sim -bM, \tag{8}$$

where $N(>M)$ is the number of earthquakes with magnitude greater than M occurring in a specified area and time and the coefficient b, called "the b value", is the negative slope of $\log N(>M)$ vs. M diagram.

A model for EQ dynamics based on a non-extensive Tsallis formalism, starting from fundamental principles, has been recently introduced by Sotolongo-Costa and Posadas (2004) and revised by Silva et al. (2006). This approach leads to a non-extensive

NHESSD
2, 2981–3013, 2014

Gutenberg–Richter type law for the magnitude distribution of EQs:

$$\log[N(>M)] = \log N + \left(\frac{2-q}{1-q}\right)\log\left[1-\left(\frac{1-q}{2-q}\right)\left(\frac{10^{2M}}{\alpha^{2/3}}\right)\right], \quad (9)$$

where N is the total number of EQs, $N(>M)$ the number of EQs with magnitude larger than M, $M \sim \log\varepsilon$. α is the constant of proportionality between the EQ energy, ε, and the size of fragment, r, ($\varepsilon \sim r^3$). It is reminded that the entropic index q characterizes the degree of non-extensivity. Importantly, the associated with Eq. (9) q values for different regions (faults) in the world are restricted in the region 1.6–1.7 (Silva et al., 2006).

The q parameter included in the non-extensive formula of Eq. (9) is associated with the b value by the relation (Sarlis et al., 2010):

$$b_{\text{est}} = 2\cdot\frac{2-q}{q-1} \quad (10)$$

In order to further verify the compliance of the analyzed EM recordings to the LRCS model, we check whether the B values typically reduce prior to large avalanches while the H values increase. Towards this direction the Gutenberg–Richter law and its non-extensive variant were employed. Both of them were applied using the notion of fracto-electromagnetic emission event, or "electromagnetic earthquake" (EM-EQ), within the frame of the self-affine nature of fracture and faulting. Within this frame, a fracto-electromagnetic emission event is considered to correspond to a fracture event which is regarded as analogous to an EQ at the geophysical scale. If $A(t_i)$ refers to the amplitude of the pre-EQ EM time-series, we regard as amplitude of a candidate "fracto-electromagnetic emission" the difference $A_{\text{fem}}(t_i) = A(t_i) - A_{\text{noise}}$, where A_{noise} is the maximum value of the EM recording during a quiet period, namely far from the time of the EQ occurrence. We consider that a sequence of k successively emerged "fracto-electromagnetic emissions" $A_{\text{fem}}(t_i)$, $i = 1,\ldots,k$ represents the EM energy released, ε,

NHESSD
2, 2981–3013, 2014

during the damage of a fragment. We shall refer to this as an "electromagnetic earthquake" (EM-EQ). Since the sum of the squared amplitude of the fracto-electromagnetic emissions is proportional to their energy, the magnitude M of the candidate EM-EQ is given by the relation $M \sim \log \varepsilon = \log\left(\sum [A_{\text{fem}}(t_i)]^2\right)$.

Both frequency–size laws were fitted in the time domain, on three large parts of the signal in order to ensure adequate statistics for the analysis. For the Gutenberg–Richter law, the fitting had a correlation coefficient $r^2 > 0.99$ for all three cases, while for its non-extensive variant a fitting error $< 1\,\%$ was achieved.

From Fig. 4 it is apparent that both methods reveal a sudden drop of b value during the two strong EM emissions, during which Hurst exponent was suddenly raised. Therefore, the analyzed EM recordings could be said to be compliant to the LRCS model. The lowering of the corresponding b values indicates the increase of the number of large events against the number of small ones.

The sudden reduction of b value is a scale-invariant precursor of an impending rupture. Indeed, during the deformation of rock in laboratory experiments, small cracking events emerge which radiate elastic waves in a manner similar to EQ (Scholz, 1968; Ponomarev et al., 1997). These emissions were found to obey the Gutenberg–Richter type relation. Acoustic Emissions (AE) from rock fracturing present a significant fall of the observed b values as the main event approaches, i.e., indicate a significant decrease in the level of the observed b values immediately before the critical point (e.g. Mogi, 1962; Scholz, 1968; Weeks et al., 1978; Ponomarev et al., 1997; Lei and Satoh, 2007; Li et al., 2009; Carpinteri et al., 2009a). The sudden reduction of the b value before the EQ occurrence is also reported at seismicity scale by several researchers (e.g. Enescu and Ito, 2001; Lu et al., 2005; Tsukakoshi and Shimazaki, 2008; Wu et al., 2008). Moreover, it is widely known that FD is directly proportional to the b value (Lu et al., 2005). Therefore, a sudden reduction of FD and b value is observed at all three scales (laboratory, fault, seismicity).

NHESSD
2, 2981–3013, 2014

3.4 Revealed physical pictures in view of the scalogram

The physical pictures outlined by the presented results are further enhanced by the time-scale analysis of the pre-EQ signal. The morlet scalogram of the signal under analysis is depicted in Fig. 5. It has to be mentioned that although a morlet wavelet was used, on the basis of its popularity, for the presented scalogram, nine mother wavelet cases were investigated, namely: morlet, meyer, mexican hat, haar, as well as different orders of coiflets, daubechies and symlets wavelets, all of them resulting to very much the same time-scale representation.

We observe on Fig. 5 that during the two strong EM bursts, the EM emission extends to all scales. However, the higher part of the emitted energy is localized to the lower frequencies. Therefore, one could conclude that the underlying fracture phenomenon extends to all fracture scales in a coherent way but with a preference to large scale fractures. This is in agreement to the physical picture resulting from the temporal evolution of the β exponent values, as indicated by the temporal evolution of Hurst exponent Fig. 2d, taking into account Eq. (4). The β exponent is shifted to higher values in the tail of the EM emission indicating the formation of a long-term memory in the system. Moreover, the FD values resulted from the Hurst exponent estimations are not only compatible with the fBm model of fracture but also with the increase of β, the reduction of b value, and all the above physical pictures. Indeed, these FD values are interrelated to Hurst exponent and β within the frame of fBm model (Eqs. 4–7), while the verified anticorrelated relation between H exponent and b value according to the LRCS model provides a linkage between FD and b value behavior. The physical picture behind this linkage is the following: the sudden reduction of the FD values observed during the two strong EM bursts implies the sudden domination of large events over the small ones since this is expected to match up to a more incomplete "fill" of space (larger entities leave more space between them than smaller ones) and it is reflected to the lower filling capacity (lower FD) of the corresponding time-series on the amplitude-time plane.

NHESSD
2, 2981–3013, 2014

All the above physical pictures are compatible to the final stage of the activation of a fault.

3.5 Fuzzy entropy

Fuzzy entropy (FuzzyEn) (Chen et al., 2007, 2009), like its ancestors approximate entropy (ApEn) and sample entropy (SampleEn) (Chen et al., 2009), is a "regularity statistics" that quantifies the unpredictability of fluctuations in a time series. For the calculation of FuzzyEn, vectors' similarity is defined by fuzzy similarity degree based on fuzzy membership functions and vectors' shapes. The gradual and continuous boundaries of fuzzy membership functions lead to a series of advantages like the continuity as well as the validity of FuzzyEn at small parameters, higher accuracy, stronger relative consistency and less dependence on data length. FuzzyEn can be considered as an upgraded alternative of SampEn (and ApEn) for the evaluation of complexity, especially for short time series contaminated by noise.

FuzzyEn calculations were performed according to the algorithm provided in (Chen et al., 2009), on successive non-overlapping 1024 samples long windows, and running time average of four windows with 25 % overlapping. It is noted that for the calculation of FuzzyEn, the exponential function has been used as the fuzzy membership function, $\mu\left(d_{ij}^{m}, R\right) = \exp\left(-\left(d_{ij}^{m}/R\right)^{n}\right)$, with $n = 2$, for $m = 2$ and $R = 0.65 \cdot \mathrm{STD}$, where STD is the standard deviation of the analyzed time-series fragment, allowing fragments with different amplitudes to be compared.

From Fig. 6 it can be observed that lower entropy values, compared to that of the background noise, can be observed between the green (left) and the red (right) broken vertical lines, although sparsely distributed in time. On the other hand, the entropy values suddenly drop during the two strong EM pulses signifying a different behavior, a new distinct phase in the tail of the EQ preparation process which is characterized by a significantly higher degree of organization and lower complexity in comparison to that of the preceding phase.

NHESSD
2, 2981–3013, 2014

This final phase of precursory EM phenomenon combines a sudden drop of entropy and a sudden drop of FD (see Fig. 3), a combination of precursory signs which have been reported by Lu et al. (2005) as a quantitative measure of the damage localization (or the clustering degree of microcracks/voids), and a likely precursor prior to a final catastrophic failure.

4 Conclusions

In this contribution, we focused on the sudden drop of fractal dimension and entropy, along with the anticorrelated, for large system sizes, rising of Hurst exponent and drop of a frequency–size power-law scaling exponent. These have been indicated as precursory signs of an impending failure by theoretical, numerical studies along with laboratory experiments. We analyzed fracto-electromagnetic emissions resulting from the activation of a single fault proving that all these signs are included in these emissions, further supporting the concept of the self-affine nature of faulting and fracture.

References

Aggelis, D. G., Soulioti, D. V., Sapouridis, N., Barkoula, N. M., Paipetis, A. S., and Matikas, T. E.: Acoustic emission characterization of the fracture process in fibre reinforced concrete, Constr. Build. Mater., 25, 4126–4131, 2011.

Bahat, D., Rabinovitch, A., and Frid, V.: Tensile Fracturing in Rocks, Springer, New York, 2005.

Bouchaud, E.: Scaling properties of cracks, J. Phys.: Condens. Matter, 9, 4319, doi:10.1088/0953-8984/9/21/002, 1997.

Buldyrev, S. V., Goldberger, A. L., Havlin, S., Mantegna, R. N., Matsa, M. E., Peng, C.-K., Simons, M., and Stanley, H. E.: Long-range correlation properties of coding and noncoding DNA sequences: GenBank analysis, Phys. Rev. E, 51, 5084–5091, 1995.

Carpinteri, A., Lacidogna, G., and Puzzi, S.: From criticality to final collapse: evolution of the "b-value" from 1.5 to 1.0, Chaos Soliton. Fract., 41, 843–853, doi:10.1016/j.chaos.2009.03.165, 2009a.

NHESSD
2, 2981–3013, 2014

Carpinteri, A., Lacidogna, G., and Niccolini, G.: Fractal analysis of damage detected in concrete structural elements under loading, Chaos Soliton. Fract., 42, 2047–2056, doi:10.1016/j.chaos.2009.03.165, 2009b.
Chen, C.-C., Lee, Y.-T., Hasumi, T., and Hsu, H.-L.: Transition on the relationship between fractal dimension and Hurst exponent in the long-range connective sandpile models, Phys. Lett. A, 375, 324–328, doi:10.1016/j.physleta.2010.11.021, 2011.
Chen, W., Wang, Z., Xie, H., and Yu, W.: Characterization of surface EMG signal based on fuzzy entropy, IEEE T. Neur. Sys. Reh., 15, 266–272, 2007.
Chen, W., Zhuang, J., Yu, W., and Wang, Z.: Measuring complexity using FuzzyEn, ApEn, and SampEn, Med. Eng. Phys., 31, 61–68, 2009.
Contoyiannis, Y. F., Kapiris, P. G., and Eftaxias, K. A.: Monitoring of a pre-seismic phase from its electromagnetic precursor, Phys. Rev. E, 71, 066123, doi:10.1103/PhysRevE.71.066123, 2005.
Cowie, P., Vanneste, C., and Sornette, D.: Statistical physics model for spatio-temporal evolution of faults, J. Geophys. Res., 98, 21809–21821, 1993.
Cowie, P., Sornette, D., and Vanneste, C.: Multifractal scaling properties of a growing fault population, Geophys. J. Int., 122, 457–469, 1995.
Eftaxias, K.: Are there pre-seismic electromagnetic precursors? A multidisciplinary approach, in: Earthquake Research and Analysis – Statistical Studies, Observations and Planning, InTech, March, doi:10.5772/28069, 460 pp., 2012.
Eftaxias, K. and Potirakis, S. M.: Current challenges for pre-earthquake electromagnetic emissions: shedding light from micro-scale plastic flow, granular packings, phase transitions and self-affinity notion of fracture process, Nonlin. Processes Geophys., 20, 771–792, doi:10.5194/npg-20-771-2013, 2013.
Eftaxias, K., Kapiris, P., Polygiannakis, J., Bogris, N., Kopanas, J., Antonopoulos, G., Peratzakis, A., and Hadjicontis, V.: Signature of pending earthquake from electromagnetic anomalies, Geophys. Res. Lett., 28, 3321–3324, 2001.
Eftaxias, K., Kapiris, P., Dologlou, E., Kopanas, J., Bogris, N., Antonopoulos, G., Peratzakis, A., and Hadjicontis, 2002 EM anomalies before the Kozani earthquake: a study of their behavior through laboratory experiments, Geophys. Res. Lett., 29, 1228, doi:10.1029/2001GL013786, 2002.

NHESSD
2, 2981–3013, 2014

Eftaxias, K., Potirakis, S. M., and Chelidze, T.: On the puzzling feature of the silence of precursory electromagnetic emissions, Nat. Hazards Earth Syst. Sci., 13, 2381–2397, doi:10.5194/nhess-13-2381-2013, 2013.

Enescu, B. and Ito, K.: Some premonitory phenomena of the 1995 Hyogo-ken Nanbu (Kobe) earthquake, Tectonophysics, 338, 297–314, 2001.

Frankel, A.: High-frequency spectral falloff of earthquakes, fractal dimension of complex rupture, *b* value, and the scaling of strength on faults, J. Geophys. Res., 96, 6291–6302, doi:10.1029/91JB00237, 1991.

Fukui, K., Okubo, S., and Terashima, T.: Electromagnetic radiation from rock during uniaxial compression testing: the effects of rock characteristics and test conditions, Rock Mech. Rock Eng., 38, 411–423, doi:10.1007/s00603-005-0046-7, 2005.

Girard, L., Weiss, J., and Amitrano, D.: Damage-cluster distribution and size effect on strength in compressive failure, Phys. Rev. Lett., 108, 225502, doi:10.1103/PhysRevLett.108.225502, 2012.

Gokhberg, M., Morgunov, V., and Pokhotelov, O.: Earthquake Prediction, Seismo-Electromagnetic Phenomena, Gordon and Breach Publishers, Amsterdam, 1995.

Guarino, A., Ciliberto, S., Garcimartín, A., Zei, M., and Scorretti, R.: Failure time and critical behaviour of fracture precursors in heterogeneous materials, Eur. Phys. J. B, 26, 141–151, doi:10.1140/epjb/e20020075, 2002.

Gutenberg, B. and Richter, C.: Seismicity of the Earth and Associated Phenomena, 2nd edn., Princeton Univ. Press, Princeton, 1954.

Hadjicontis, V., Mavromatou, C., Antsygina, T. N., and Chishko, K. A.: Mechanism of electromagnetic emission in plastically deformed ionic crystal, Phys. Rev. B, 76, 024106, doi:10.1103/PhysRevB.76.024106, 2007.

Hadjicontis, V., Mavromatou, C., Mastrogiannis, D., Antsygina, T. N., and Chishko, K. A.: Relationship between electromagnetic and acoustic emissions during plastic deformation of gamma-irradiated LiF monocrystals, J. Appl. Phys., 110, 024907, doi:10.1063/1.3608247, 2011.

Hallgass, R., Loreto, V., Mazzella, O., Paladin, G., and Pietronero, L.: Earthquake statistics and fractal faults, Phys. Rev. E, 56, 1346–1356, 1997.

Hansen, A. and Schmittbuhl, J.: Origin of the universal roughness exponent of brittle fracture surfaces: stress-weighted percolation in the damage zone, Phys. Rev. Lett., 90, 045504, doi:10.1103/PhysRevLett.90.045504, 2003.

NHESSD

2, 2981–3013, 2014

Hayakawa, M.: Atmospheric and Ionospheric Electromagnetic Phenomena Associated with Earthquakes, Terrapub, Tokyo, 1999.
Hayakawa, M. and Fujinawa, Y.: Electromagnetic Phenomena Related to Earthquake Prediction, Terrapub, Tokyo, 1994.
Heneghan, C. and McDarby, G.: Establishing the relation between detrended fluctuation analysis and power spectral density analysis for stochastic processes, Phys. Rev. E, 62, 6103–6110, 2000.
Herrmann, H. J. and Roux, S.: Statistical Models for Fracture and Disordered Media, North-Holland, Amsterdam, 1990.
Houle, P. A. and Sethna, J. P.: Acoustic emission from crumpling paper, Phys. Rev. E, 54, 278–283, 1996.
Hurst, H.: Long term storage capacity of reservoirs, T. Am. Soc. Civ. Eng., 116, 770–808, 1951.
Kalimeri, M., Papadimitriou, C., Balasis, G., and Eftaxias, K.: Dynamical complexity detection in pre-seismic emissions using nonadditive Tsallis entropy, Physica A, 387, 1161–1172, 2008.
Kapiris, P. G., Eftaxias, K. A., and Chelidze, T. L.: Electromagnetic signature of prefracture criticality in heterogeneous media, Phys. Rev. Lett., 92, 065702, doi:10.1103/PhysRevLett.92.065702, 2004a.
Kapiris, P. G., Balasis, G. T., Kopanas, J. A., Antonopoulos, G. N., Peratzakis, A. S., and Eftaxias, K. A.: Scaling similarities of multiple fracturing of solid materials, Nonlin. Processes Geophys., 11, 137–151, doi:10.5194/npg-11-137-2004, 2004b.
Karamanos, K., Dakopoulos, D., Aloupis, K., Peratzakis, A., Athanasopoulou, L., Nikolopoulos, S., Kapiris, P., and Eftaxias, K.: Study of pre-seismic electromagnetic signals in terms of complexity, Phys. Rev. E, 74, 016104, doi:10.1103/PhysRevE.74.016104, 2006.
Krajcinovic, D.: Damage Mechanics, Elsevier, Amsterdam, 1996.
Kuksenko, V. S., Damaskinskaya, E. E., and Kadomtsev, A. G.: Fracture of granite under various strain conditions, Izvestiya, Physics of the Solid Earth, 47, 879–885, 2011.
Lacidogna, G., Manuello, A., Carpinteri, A., Niccolini, G., Agosto, A., and Durin, G.: Acoustic and electromagnetic emissions in rocks under compression, in: Proceeding of the SEM Annual Conference 2010, Indianapolis, Indiana, USA, 2010, Society for experimental Mechanics Inc., 2010.
Lacidogna, G., Carpinteri, A., Manuello, A., Durin, G., Schiavi, A., Niccolini, G., and Agosto, A.: Acoustic and electromagnetic emissions as precursor phenomena in failure processes, Strain, 47, 144–152, doi:10.1111/j.1475-1305.2010.00750.x, 2011.

NHESSD
2, 2981–3013, 2014

Lavrov, A.: Fracture-induced physical phenomena and memory effects in rocks: a review, Strain, 41, 135–149, 2005.
Lee, Y.-T., Chen, C.-C., Hasumi, T., and Hsu, H.-L.: Precursory phenomena associated with large avalanches in the long-range connective sandpile model II: an implication to the relation between the *b*-value and the Hurst exponent in seismicity, Geophys. Res. Lett., 36, L02308, doi:10.1029/2008GL036548, 2009.
Lee, Y.-T., Chen, C.-C., Lin, C.-Y., and Chi, S.-C.: Negative correlation between power-law scaling and Hurst exponents in long-range connective sandpile models and real seismicity, Chaos Solit. Fract., 45, 125–130, 2012.
Lei, X.-L., and Satoh, T.: Indicators of critical point behavior prior to rock failure inferred from pre-failure damage, Tectonophysics, 431, 97–111, doi:10.1016/j.tecto.2006.04.023, 2007.
Li, Y. H., Liu, J.-P., Zhao, X.-D., and Yang, Y.-J.: Study on *b*-value and fractal dimension of acoustic emission during rock failure process, Rock and Soil Mech., 30, 2559–2563, 2009.
Lomnitz, C.: Fundamentals of Earthquake Prediction, John Wiley & Sons, Inc, New York, 1994.
Lopez, J. M. and Schmittbuhl, J.: Anomalous scaling of fracture surfaces, Phys. Rev. E, 57, 6405–6408, 1998.
Lowen, S. B. and Teich, M. C.: Estimation and simulation of fractal stochastic point processes, Fractals, 3, 183–210, 1995.
Lu, C., Mai, Y.-W., and Xie, H.: A sudden drop of fractal dimension: a likely precursor of catastrophic failure in disordered media, Phil. Mag. Lett., 85, 33–40, 2005.
Maes, C., VanMoffaert, A., Frederix, H., and Strauven, H.: Criticality in creep experiments on cellular glass, Phys. Rev. B, 57, 4987–4990, 1998.
Mandelbrot, B. B.: The Fractal Geometry of Nature, Freeman, New York, 1983.
Mandelbrot, B. B. and Wallis, J. R.: Noah, Joseph and operational hydrology, Water Resour. Res., 4, 909–918, 1968.
Matsumoto, H., Ikeya, M., and Yamanaka, C.: Analysis of barberpole color and speckle noises recorded 6 and half hours before the Kobe earthquake, Jpn. J. Appl. Phys., 37, 1409–1411, 1998.
Mogi, K.: Magnitude frequency relation for elastic shocks accompanying fractures of various materials and some related problems in earthquakes, B. Earthq. Res. I. Tokyo Univ., 40, 831–853, 1962.
Morgounov, V.: Relaxation creep model of impending earthquake, Ann. Geophys., 44, 369–381, doi:10.4401/ag-3603, 2001.

NHESSD
2, 2981–3013, 2014

Mori, Y. and Obata, Y.: Electromagnetic emission and AE Kaiser effect for estimating rock in-situ stress, Report of the Research Institute of Industrial Technology Nihon University, 93, 1–16, 2008.
Mourot, G., Morel, S., Bouchaud, E., and Valentin, G.: Scaling properties of mortar fracture surfaces, Int. J. Fracture, 140, 39–54, 2006.
Nitsan, U.: Electromagnetic emission accompanying fracture of quartz-bearing rocks, Geophys. Res. Lett., 4, 333–337, 1977.
Ohnaka, M.: Acoustic emission during creep of brittle rock, Int. J. Rock Mech. Min., 20, 121–134, 1983.
Ohnaka, M. and Mogi, K.: Frequency characteristics of acoustic emission in rocks under uniaxial compression and its relation to the fracturing process to failure, J. Geophys. Res., 87, 3873–3884, doi:10.1029/JB087iB05p03873, 1982.
Papadimitriou, C., Kalimeri, M., and Eftaxias, K.: Nonextensivity and universality in the EQ preparation process, Phys. Rev. E, 77, 036101, doi:10.1103/PhysRevE.77.036101, 2008.
Peng, C.-K., Buldyrev, S. V., Havlin, S., Simons, M., Stanley, H. E., and Goldberger, A. L.: Mosaic organization of DNA nucleotides, Phys. Rev. E, 49, 1685–1689, 1994.
Peng, C.-K., Havlin, S., Stanley, H. E., and Goldberger, A. L.: Quantification of scaling exponents and crossover phenomena in nonstationary heartbeat time series, Chaos, 5, 82–87, doi:10.1063/1.166141, 1995.
Petri, A., Paparo, G., Vespignani, A., Alippi, A., Costantini, M.: Experimental evidence for critical dynamics in microfracturing processes, Phys. Rev. Lett., 73, 3423, doi:10.1103/PhysRevLett.73.3423, 1994.
Ponomarev, A., Zavyalov, A., Smirnov, V., and Lockner, D.: Physical modelling of the formation and evolution of seismically active fault zones, Tectonophysics, 277, 57–81, 1997.
Ponson, L., Bonamy, D., and Bouchaud, E.: Two-dimensional scaling properties of experimental fracture surfaces, Phys. Rev. Lett., 96, 035506, doi:10.1103/PhysRevLett.96.035506, 2006.
Potirakis, S. M., Minadakis, G., and Eftaxias, K.: Analysis of electromagnetic pre-seismic emissions using Fisher information and Tsallis entropy, Physica A, 391, 300–306, doi:10.1016/j.physa.2011.08.003, 2012a.
Potirakis, S. M., Minadakis, G., and Eftaxias, K.: Relation between seismicity and pre-earthquake electromagnetic emissions in terms of energy, information and entropy content, Nat. Hazards Earth Syst. Sci., 12, 1179–1183, doi:10.5194/nhess-12-1179-2012, 2012b.

NHESSD
2, 2981–3013, 2014

Potirakis, S. M., Minadakis, G., and Eftaxias, K.: Sudden drop of fractal dimension of electromagnetic emissions recorded prior to significant earthquake, Nat. Hazards, 64, 641–650, doi:10.1007/s11069-012-0262-x, 2012c.
Rabinovitch, A., Frid, V., and Bahat, D.: Gutenberg–Richter-type relation for laboratory fracture-induced electromagnetic radiation, Phys. Rev. E, 65, 011401, doi:10.1103/PhysRevE.65.011401, 2001.
Raghavendra, B. S. and Narayana Dutt, D.: Computing fractal dimension of signals using multiresolution box-counting method, World Acad. of Sci., Eng., and Technol., 61, 1223–1238, 2010.
Rundle, J. B., Turcotte, D. L., Shcherbakov, R., Klein, W., and Sammis, C.: Statistical physics approach to understanding the multiscale dynamics of earthquake fault systems, Rev. Geophys., 41, 1019, doi:10.1029/2003RG000135, 2003.
Sahimi, M.: Flow phenomena in rocks: from continuum models to fractals, percolation, cellular automata, and simulated annealing, Rev. Mod. Phys., 65, 1393–1534, 1993.
Sahimi, M. and Tajer, S. E.: Self-affine fractal distributions of the bulk density, elastic moduli, and seismic wave velocities of rock, Phys. Rev. E, 71, 046301, doi:10.1103/PhysRevE.71.046301, 2005.
Sahimi, M., Robertson, M. C., and Sammis, C. G.: Fractal distribution of earthquakes hypocenters and its relation to fault patterns and percolation, Phys. Rev. Lett., 70, 2186–2189, 1993.
Sarlis, N. V., Skordas, E. S., and Varotsos, P. A.: Nonextensivity and natural time: the case of seismicity, Phys. Rev. E, 82, 021110, doi:10.1103/PhysRevE.82.021110, 2010.
Schmittbuhl, J., Vilotte, J. P., and Roux, S.: Reliability of self-affine measurements, Phys. Rev. E, 51, 131–147, 1995.
Scholz, C. H.: The frequency–magnitude relation of microfracturing in rock and its relation to earthquakes, B. Seismol. Soc. Am., 58, 399–415, 1968.
Schiavi, A., Niccolini, G., Terrizzo, P., Carpinteri, A., Lacidogna, G., and Manuello, A.: Acoustic emissions at high and low frequencies during compression tests in brittle materials, Strain, 47, 105–110, 2011.
Shadkhoo, S., Ghanbarnejad, F., Jafari, G. R., and Tabar, M. R. R.: Scaling behavior of earthquakes' inter-events time series, Cent. Eur. J. Phys., 7, 620–623, 2009.
Sharon, E. and Fineberg, J.: Confirming the continuum theory of dynamic brittle fracture for fast cracks, Nature, 397, 333, doi:10.1038/16891, 1999.

NHESSD
2, 2981–3013, 2014

Silva, R., Franca, G. S., Vilar, C. S., and Alcaniz, J. S.: Nonextensive models for earthquakes, Phys. Rev. E, 73, 026102, doi:10.1103/PhysRevE.73.026102, 2006.
Sornette, D.: Self-organized criticality in plate tectonics, in: Spontaneous Formation of Space–Time Sructures and Criticality, edited by: Riste, T. and Sherrington, D., Kluwer Academic Publishers, Dordrecht, 57–106, 1991.
Sornette, D.: Critical phenomena in natural sciences, in: Chaos, Fractals, Selforganization and Disorder: Concepts and Tools, Springer, Berlin, Heidelberg, New York, 2000.
Sornette, D., Miltenberger, P., and Vanneste, C.: Statistical physics of fault patterns self-organized by repeated earthquakes, Pure Appl. Geophys., 142, 491–527, 1994.
Sotolongo-Costa, O. and Posadas, A.: Fragment-asperity interaction model for earthquakes, Phys. Rev. Lett., 92, 048501, doi:10.1103/PhysRevLett.92.048501, 2004.
Soulioti, D., Barkoula, N. M., Paipetis, A., Matikas, T. E., Shiotani, T., and Aggelis, D. G.: Acoustic emission behavior of steel fibre reinforced concrete under bending, Constr. Build. Mater., 23, 3532–3536, 2009.
Tsukakoshi, Y. and Shimazaki, K.: Decreased b-value prior to the *M* 6.2 Northern Miyagi, Japan, earthquake of 26 July 2003, Earth Planets Space, 60, 915–924, 2008.
Uyeda, S.: Short-term earthquake prediction: current status of seismo-electromagnetics, Tectonophysics, 470, 205–213, 2009.
Vettegren, V. I., Kuksenko, V. S., Mamalimov, R. I., and Shcherbakov, I. P.: Dynamics of fractoluminescence, electromagnetic and acoustic emissions upon impact on a granite surface, Izvestiya, Physics of the Solid Earth, 48, 415–420, 2012.
Warwick, J. W., Stoker, C., and Meyer, T. R.: Radio emission associated with rock fracture: possible application to the great Chilean earthquake of May 22 1960, J. Geophys. Res., 87, 2851–2859, 1982.
Weeks, J., Lockner, D., and Byerlee, J.: Changes in b-values during movement on cut surfaces in granite, B. Seismol. Soc. Am., 68, 333–341, 1978.
Wu, Y.-M., Chen, C.-C., Zhao, L., and Chang, C.-H.: Seismicity characteristics before the 2003 Chengkung, Taiwan, earthquake, Tectonophysics, 457, 177–182, 2008.
Zapperi, S., Nukala, P., and Simunovic, S.: Crack roughness and avalanche precursors in the random fuse model, Phys. Rev. E, 71, 026106, doi:10.1103/PhysRevE.71.026106, 2005.

NHESSD
2, 2981–3013, 2014

Table 1. List of acronyms/abbreviations.

Acronym/Abbreviation	Description
EQ	Earthquake
FD	Fractal Dimension
LRCS	Long-range connective sandpile
SAM	Self-affine model
EM	Electromagnetic
DFA	Detrended fluctuation analysis
R/S	Rescaled-range analysis
FuzzyEn	Fuzzy entropy
UT	Universal Time (Greenwich Mean Time)
fBm	fractional Brownian motion
EM-EQ	"Electromagnetic earthquake"
SampEn	Sample entropy
ApEn	Approximate entropy

NHESSD
2, 2981–3013, 2014

Table 2. List of symbrols.

Symbol	Description
B	Frequency–size power-law scaling exponent used in long-range connective sandpile models
H	Hurst exponent
b	Gutenberg–Richter frequency–size power-law scaling exponent
ε	Energy released during an earthquake or electromagnetic energy released during the damage of a fragment
γ	Power law exponent of the probability of an earthquake releasing an energy E
d	Geometric dimension
m	Sample length (number of samples) of a time-series
$F(m)$	Root mean-square fluctuation for the integrated and detrended series
a	DFA scaling exponent
f	Frequency
$S(f)$	Power spectral density
β	Spectral power law exponent
r^2	Linear correlation coefficient
H_a	Estimated Hurst exponent, under the fBm hypothesis, from the calculated DFA exponent a (using Eq. 5)
H_β	Estimated Hurst exponent, under the fBm hypothesis, from the calculated spectral scaling exponent β (using Eq. 4)
D	Fractal Dimension
D_h	Estimated Fractal Dimension, under the fBm hypothesis, from the directly calculated (through the R/S analysis) Hurst exponent, H, (using Eq. 7).
$D_{\mathrm{h}a}$	Estimated Fractal Dimension, under the fBm hypothesis, from the DFA estimated Hurst exponent H_a
$D_{\mathrm{h}\beta}$	Estimated Fractal Dimension, under the fBm hypothesis, from the spectral scaling estimated Hurst exponent H_β
M	Earthquake magnitude
$N(>M)$	Number of earthquakes with magnitude greater than M
r	Fragment size used in Eq. (9)
α	constant of proportionality between the EQ energy, ε, and the size of fragment, r, ($\varepsilon \sim r^3$) used in Eq. (9)
q	Non-extensive Tsallis entropic index
b_est	Estimated Gutenberg law scaling exponent (using Eq. 10)
A	Amplitude of the pre-earthquake electromagnetic time-series
A_noise	Maximum value of the electromagnetic recording during a quiet period
A_fem	Amplitude of a candidate "fracto-electromagnetic emission"
μ	Fuzzy membership function

NHESSD
2, 2981–3013, 2014

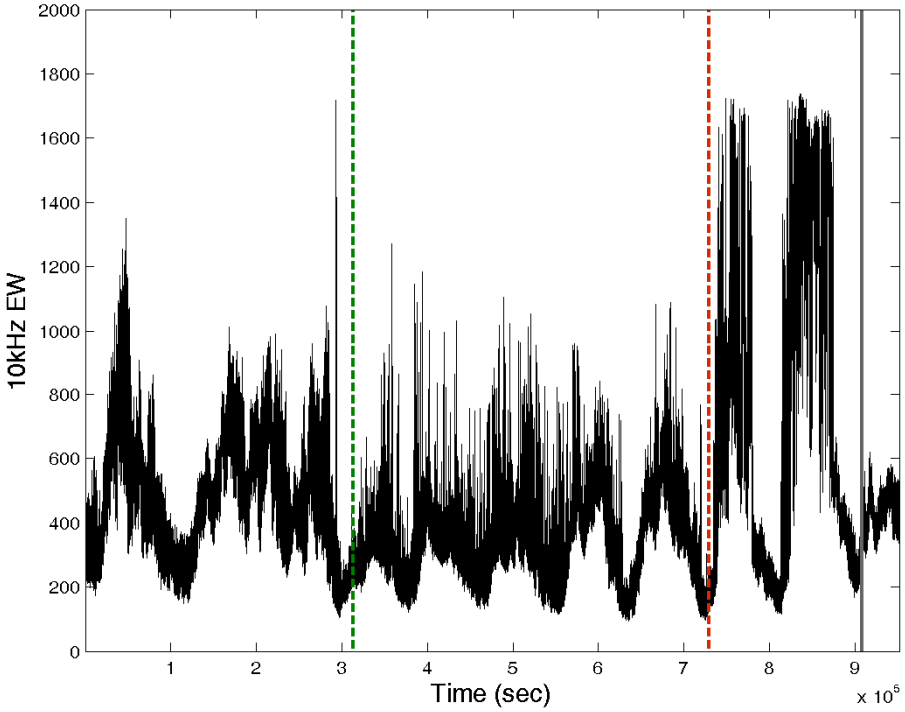

Fig. 1. Part of the recorded time series of the 10 kHz (east–west) magnetic field strength (in arbitrary units) covering 11 days period from 28 August 1999, 00:00:00 (UT), to 7 September 1999, 23:59:59 (UT), associated with the Athens EQ. The vertical solid grey line indicates the time of the Athens EQ occurrence. The (left) vertical broken green line roughly indicates the start of the candidate precursor. The (right) vertical broken red line indicates where the damage evolution of the fault approaches the critical point.

NHESSD
2, 2981–3013, 2014

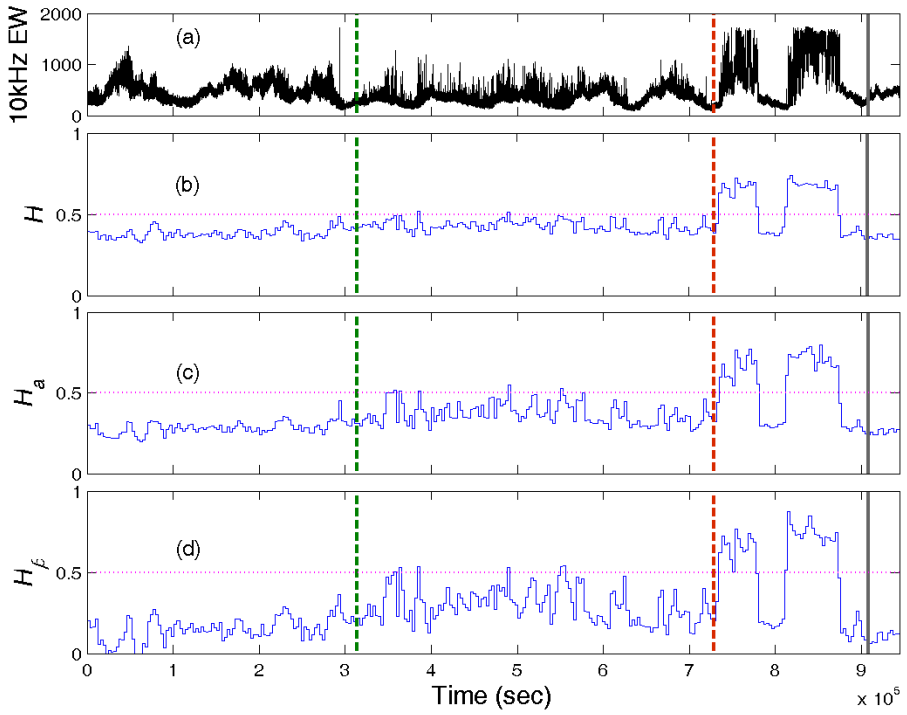

Fig. 2. (a) Part of the recorded time series of the 10 kHz (east–west) magnetic field strength (in arbitrary units) covering 11 days period from 28 August 1999, 00:00:00 (UT), to 7 September 1999, 23:59:59 (UT), associated with the Athens EQ. The corresponding variation vs. time of Hurst exponent, **(b)** H, resulting from R/S method, **(c)** H_a, estimated via DFA, and **(d)** H_β calculated from spectral power law. The common horizontal axis is the time (in s), denoting the relative time position from the beginning of the analyzed part of the EM recording. The vertical lines have the same position and meaning as in Fig. 1. (For interpretation of the references to color in this figure, the reader is referred to the online version of this article.)

NHESSD
2, 2981–3013, 2014

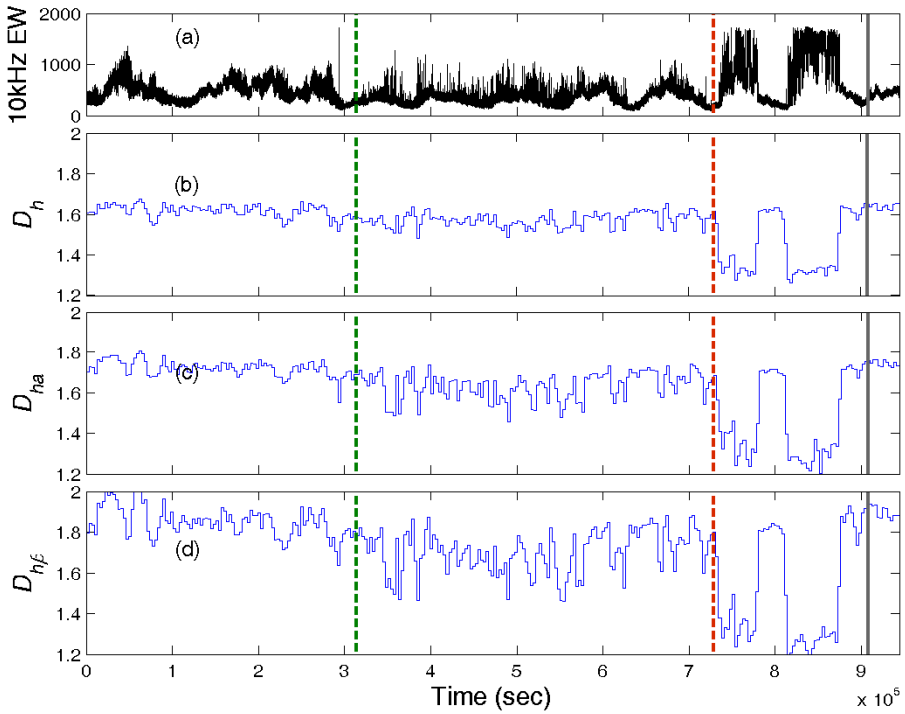

Fig. 3. (a) Part of the recorded time series of the 10 kHz (east–west) magnetic field strength (in arbitrary units) covering 11 days period from 28 August 1999, 00:00:00 (UT), to 7 September 1999, 23:59:59 (UT), associated with the Athens EQ. The corresponding temporal variation of the Hausdorff–Besicovitch FD **(b)** D_{h}, as resulting from H **(c)** D_{ha} as resulting from H_a, and **(d)** $D_{\mathrm{h}\beta}$ calculated from H_β, all calculated using Eq. (7). The common horizontal axis is the time (in s), denoting the relative time position from the beginning of the analyzed part of the EM recording. The vertical lines have the same position and meaning as in Fig. 1. (For interpretation of the references to color in this figure, the reader is referred to the online version of this article.)

NHESSD
2, 2981–3013, 2014

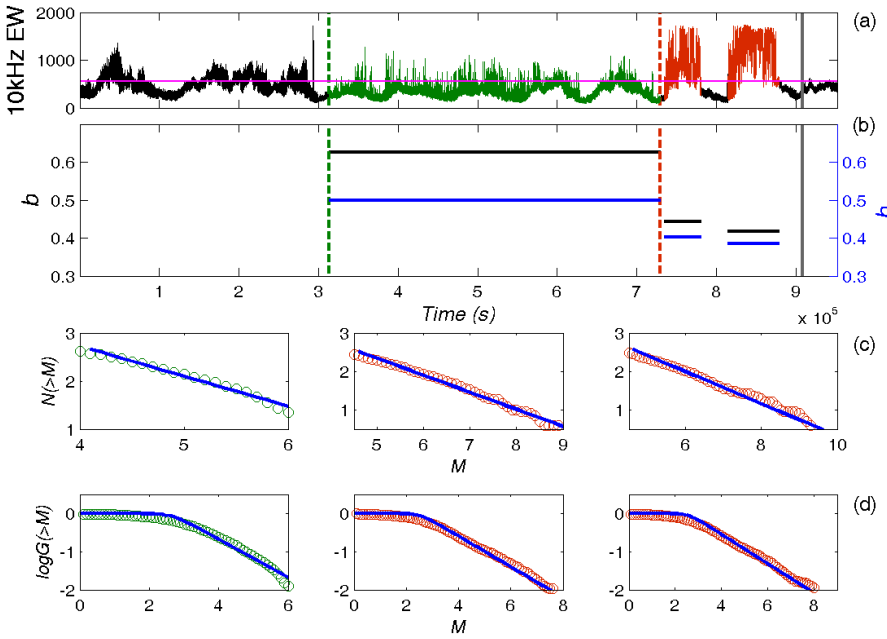

Fig. 4. (a) Part of the recorded time series of the 10 kHz (east–west) magnetic field strength (in arbitrary units) covering 11 days period from 28 August 1999, 00:00:00 (UT), to 7 September 1999, 23:59:59 (UT), associated with the Athens EQ. **(b)** Temporal variation of the b value, and the b_{est}, estimated from the non-extensive q parameter (Eq. 10). **(c)** Fitting of the Gutenberg–Richter law and **(d)** the non-extensive Gutenberg–Richter law, on the three parts of the analyzed signal (color and position correspondence from left to right). The common horizontal axis is the time (in s), denoting the relative time position from the beginning of the analyzed part of the EM recording. The magenta horizontal line on Fig. 4a indicates the noise level threshold $A_{\text{noise}} = 620$ a.u. The vertical lines have the same position and meaning as in Fig. 1. (For interpretation of the references to color in this figure, the reader is referred to the online version of this article.)

NHESSD
2, 2981–3013, 2014

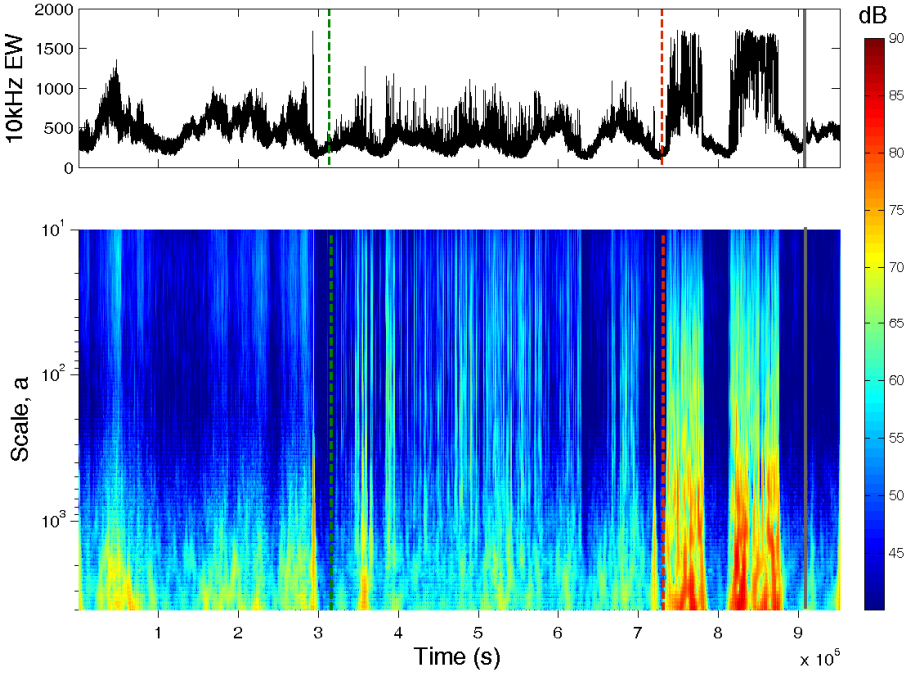

Fig. 5. (a) Part of the recorded time series of the 10 kHz (east–west) magnetic field strength (in arbitrary units) covering 11 days period from 28 August 1999, 00:00:00 (UT), to 7 September 1999, 23:59:59 (UT), associated with the Athens EQ. **(b)** The corresponding morlet wavelet scalogram, with vertical axis corresponding to the scale, *a*, of the wavelet (time scale, reciprocal to the wavelet "frequency") and color representing the power spectral level in dB (side colorbar). The common horizontal axis is the time (in s), denoting the relative time position from the beginning of the analyzed part of the EM recording. The vertical lines have the same position and meaning as in Fig. 1. (For interpretation of the references to color in this figure, the reader is referred to the online version of this article.)

NHESSD
2, 2981–3013, 2014

Signatures of the self-affinity of fracture and faulting

S. M. Potirakis et al.

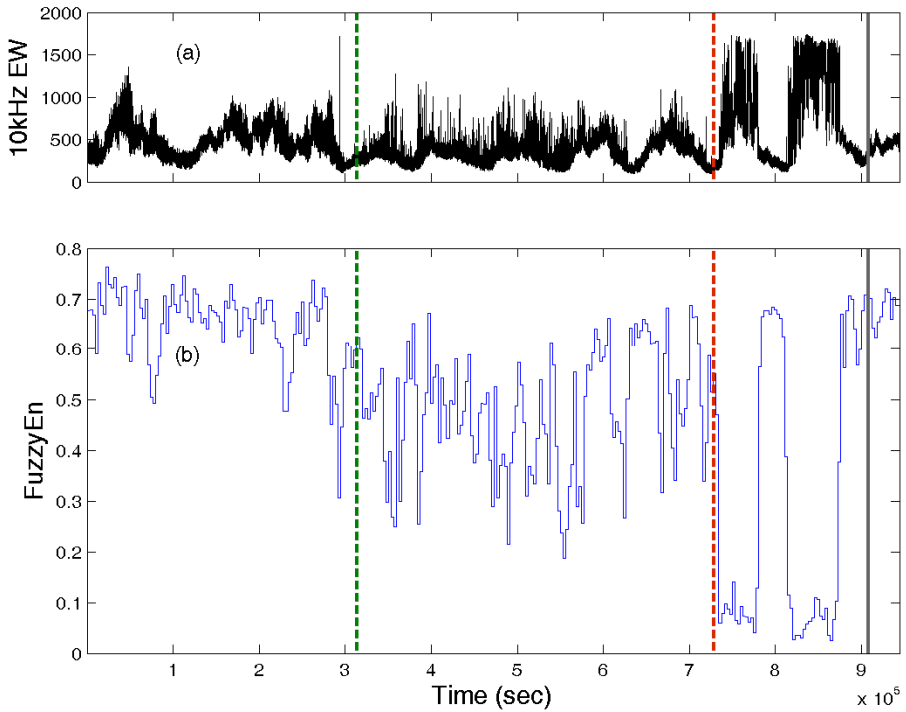

Fig. 6. (a) Part of the recorded time series of the 10 kHz (east–west) magnetic field strength (in arbitrary units) covering 11 days period from 28 August 1999, 00:00:00 (UT), to 7 September 1999, 23:59:59 (UT), associated with the Athens EQ. **(b)** The corresponding FuzzyEn. The common horizontal axis is the time (in s), denoting the relative time position from the beginning of the analyzed part of the EM recording. The vertical lines have the same position and meaning as in Fig. 1. (For interpretation of the references to color in this figure, the reader is referred to the online version of this article.)

NHESSD
2, 2981–3013, 2014